

Arbitrary-order Hilbert spectral analysis for time series possessing scaling statistics: a comparison study with detrended fluctuation analysis and wavelet leaders

Y.X. Huang (黄永祥)^{1,2,3,4,5,6,7,*} F. G. Schmitt^{8,5,6,†} J.-P. Hermand⁷ Y. Gagne⁹ Z.M. Lu (卢志明)^{1,2,3} and Y.L. Liu (刘宇陆)^{1,2}

¹Shanghai Institute of Applied Mathematics and Mechanics, Shanghai University, Shanghai 200072, China

²Shanghai Key Laboratory of Mechanics in Energy and Environment Engineering, Yanchang Road, Shanghai 200072, China

³E-Institutes of Shanghai Universities, Shanghai University, Shanghai 200072, China

⁴Université Lille Nord de France, F-59044 Lille, France

⁵USTL, LOG, F-62930 Wimereux, France

⁶CNRS, UMR 8187, F-62930 Wimereux, France

⁷Environmental Hydroacoustics Laboratory, Université Libre de Bruxelles, Avenue F.D. Roosevelt 50 - CP 194/5, B-1050 Brussels, Belgium

⁸Univ Lille Nord de France

⁹LEGI, CNRS/UJF-INPG, UMR 5519, F-38041 Grenoble, France

(Dated: October 17, 2018)

In this paper we present an extended version of Hilbert-Huang transform, namely arbitrary-order Hilbert spectral analysis, to characterize the scale-invariant properties of a time series directly in an amplitude-frequency space. We first show numerically that due to a nonlinear distortion, traditional methods require high-order harmonic components to represent nonlinear processes, except for the Hilbert-based method. This will lead to an artificial energy flux from the low-frequency (large scale) to the high-frequency (small scale) part. Thus the power law, if it exists, is contaminated. We then compare the Hilbert method with structure functions (SF), detrended fluctuation analysis (DFA), and wavelet leader (WL) by analyzing fractional Brownian motion and synthesized multifractal time series. For the former simulation, we find that all methods provide comparable results. For the latter simulation, we perform simulations with an intermittent parameter $\mu = 0.15$. We find that the SF underestimates scaling exponent when $q > 3$. The Hilbert method provides a slight underestimation when $q > 5$. However, both DFA and WL overestimate the scaling exponents when $q > 5$. It seems that Hilbert and DFA methods provide better singularity spectra than SF and WL. We finally apply all methods to a passive scalar (temperature) data obtained from a jet experiment with a Taylor's microscale Reynolds number $Re_{\lambda} \simeq 250$. Due to the presence of strong ramp-cliff structures, the SF fails to detect the power law behavior. For the traditional method, the ramp-cliff structure causes a serious artificial energy flux from the low-frequency (large scale) to the high-frequency (small scale) part. Thus DFA and WL underestimate the scaling exponents. However, the Hilbert method provides scaling exponents $\xi_{\theta}(q)$ quite close to the one for longitudinal velocity, indicating a less intermittent passive scalar field than what was believed before.

PACS numbers: 94.05.Lk, 05.45.Tp, 02.50.Fz

I. INTRODUCTION

Multifractal properties have been found in many fields, such as turbulence [1–3], rainfall [4–7], financial time series [8–11], physiology [12], etc. Conventionally, multifractal properties of such time series are characterized by the scaling exponents $\zeta(q)$, which are extracted by structure function (SF) analysis: $\Delta V_{\ell}^q \sim \ell^{\zeta(q)}$, where $\Delta V_{\ell} = |V(x + \ell) - V(x)|$ are the increment for scale separation ℓ , and $\zeta(q)$ is a nonlinear function [1, 2, 13]. The function $\zeta(q)$ is linear for monoscaling processes and nonlinear for multifractal processes. We may also mention the detrended fluctuation analysis (DFA) [14–16] or the multifractal detrended fluctuation analysis [17], which are sometimes also employed for scaling time series analysis. The DFA method is similar to SFs since it involves

increments and characterizes the scale invariance in the physical domain.

Other widely used methods are wavelet-based methods, e.g. wavelet transform modulus maxima (WTMM), wavelet leader (WL), or gradient modulus wavelet projection (GMWP), to extract the scaling exponents from a scaling time series [18–30]. However, as we will show in this paper, the wavelets share the same drawback with Fourier transform, which requires high-order harmonic components to represent nonlinear processes.

Some of us have proposed recently a new methodology, namely arbitrary-order Hilbert spectral analysis (HSA), to characterize the scale invariant properties directly in amplitude-frequency space [31–33]. It is an extended version of the Hilbert-Huang transform (HHT), which provides a joint probability density function (pdf) in an amplitude-frequency space [31, 33]. We have applied part of this new methodology to several different time series to show its efficiency and validity: turbulence experimental database [31], synthesized fractional Brownian mo-

* yongxianghuang@gmail.com

† francois.schmitt@univ-lille1.fr

tion (fBm) time series [32], surf zone marine turbulence data [34], and river flow discharge data [35]. In this paper we consider in length and precisely this new method and its validation and calibration. We first introduce this new methodology in detail. We then validate and calibrate it by analyzing a synthesized multifractal time series. We finally consider a passive scalar (temperature) data set with strong ramp-cliff structures. Due to the presence of ramp-cliff structures, the classical SF analysis fails to detect the power law behavior [36]. Additionally, for traditional methods, such as Fourier transform, wavelet transform, high-order harmonics is required to represent these structures and leads to an artificial energy flux from the large-scale part (low frequency) to the small-scale part (high frequency) [36].

This paper is organized as follows. We present the definition of the arbitrary-order Hilbert spectral analysis in Sec. II. The classical structure function analysis, multifractal detrended fluctuation analysis and wavelet leader are also presented in this section. We then consider a nonlinear effect by using the classical Duffing equation to show the artificial high-order harmonic components required by the classical methods, for example, Fourier transform, and wavelet transform, in Sec. III. In Sec. IV we perform a comparison study of the arbitrary-order HSA with other methods by analyzing a fBm simulation and a synthesized multifractal time series. We then present in Sec. V an analysis of real temperature data obtained from a jet experiment. We finally draw the main conclusions in Sec. VI.

II. METHODOLOGY

A. Arbitrary-order Hilbert spectral analysis

1. Empirical mode decomposition

The most innovative part of the Hilbert-Huang transform is the so-called empirical mode decomposition (EMD). In the real world most of the signals are multi-components, which means that different scales can co-exist simultaneously [37–39]. This may be considered as fast oscillations superposed to slower ones at a local level [40, 41]. Meanwhile, for decomposition methods, a characteristic scale (CS) is always defined implicitly or explicitly before the decomposition. For example, the CS of the classical Fourier analysis is a period of sine wave. The CS of wavelet transform is the shape of the mother wavelet [33]. In the present method, the CS is defined as the distance between two successive maxima (respectively minima) points. Then the so-called intrinsic mode functions (IMF) are proposed to represent each mono-component signal. An IMF satisfies the following two conditions: (i) the difference between the number of local extrema and the number of zero-crossings must be zero or one; (ii) the running mean value of the envelope defined by the local maxima and the envelope defined by

the local minima is zero [38, 39].

A subpart of the EMD algorithm, called “sifting process,” is then designed to decompose a given signal into several IMF modes [38–40]. The first step of the sifting process is to identify all the local maxima (respectively, minima) points for a given time series $x(t)$. Once all the local extrema points are identified, the upper envelope $e_{\max}(t)$ and the lower envelope $e_{\min}(t)$ are constructed, respectively, for the local maxima and minima points by using a cubic spline algorithm. The mean between these two envelopes is defined as

$$m_1(t) = \frac{e_{\max}(t) + e_{\min}(t)}{2} \quad (1)$$

Thus the first component is estimated by

$$h_1(t) = x(t) - m_1(t) \quad (2)$$

Ideally, $h_1(t)$ should be an IMF as expected. However, $h_1(t)$ may not satisfy the above-mentioned conditions to be an IMF. The function $h_1(t)$ is then taken as a new time series and this sifting process is repeated j times, until $h_{1j}(t)$ is an IMF

$$h_{1j}(t) = h_{1(j-1)}(t) - m_{1j}(t) \quad (3)$$

The first IMF component $C_1(t)$ is then written as

$$C_1(t) = h_{1j}(t) \quad (4)$$

and the residual $r_1(t)$ as

$$r_1(t) = x(t) - C_1(t) \quad (5)$$

from the data $x(t)$. The sifting procedure is then repeated on the residual until $r_n(t)$ becomes a monotonic function or at most has one local extreme point, which means that no more IMF can be extracted from $r_n(t)$. There are finally $n - 1$ IMF modes with one residual $r_n(t)$. The original signal $x(t)$ is rewritten at the end of the process as

$$x(t) = \sum_{i=1}^{n-1} C_i(t) + r_n(t) \quad (6)$$

To guarantee that the IMF modes retain enough physical sense, a certain stopping criterion has to be introduced to stop the sifting process properly. Different types of stopping criteria have been introduced by several authors [38–40, 42, 43]. The first stopping criterion is a Cauchy-type convergence criterion. We introduce the standard deviation (SD), defined for two successive sifting processes as

$$\text{SD} = \frac{\sum_{t=0}^T |h_{i(j-1)}(t) - h_j(t)|^2}{\sum_{t=0}^T h_{i(j-1)}^2(t)} \quad (7)$$

If a calculated SD is smaller than a given value, then the sifting stops, and gives an IMF. A typical value is

141 0.2 ~ 0.3, proposed based on Huang et al.'s experiences
 142 [38, 39]. Another widely used criterion is based on three
 143 thresholds α , θ_1 , and θ_2 , which are designed to guarantee
 144 globally small fluctuations meanwhile taking into account
 145 locally large excursions [40]. The mode amplitude and
 146 evaluation function are given as

$$a(t) = \frac{e_{\max}(t) - e_{\min}(t)}{2} \quad (8a)$$

147 and

$$\sigma(t) = |m(t)/a(t)| \quad (8b)$$

148 So that the sifting is iterated until $\sigma(t) < \theta_1$ for some
 149 prescribed fraction $1 - \alpha$ of the total duration, while
 150 $\sigma(t) < \theta_2$ for the remaining fraction. The typical values
 151 proposed by Rilling et al. [40] are $\alpha \approx 0.05$, $\theta_1 \approx 0.05$
 152 and $\theta_2 \approx 10\theta_1$, respectively based on their experience. In
 153 our practice, if one of these criteria is satisfied, then the
 154 sifting process will stop. We also set a maximal iteration
 155 number (e.g., 300) to avoid over-decomposing the time
 156 series.

157 The above-described EMD algorithm performs the de-
 158 composition on a very local level in the physical do-
 159 main without *a priori* basis. This means that the
 160 present decomposition is *a posteriori*: The basis is in-
 161 duced by the data itself [38, 39, 41]. It is thus a
 162 scale-based decomposition. Since its introduction, this
 163 method has attracted large interests in various research
 164 fields: waves [34, 44, 45], biological applications [46–
 165 48], financial studies [49], meteorology and climate stud-
 166 ies [35, 50–54], mechanical engineering [55, 56], acous-
 167 tics [57], aquatic environment [58], and turbulence [31], to
 168 quote a few. More detail about the EMD algorithm can
 169 be found in several methodological papers [38–41, 43, 59].

170 2. Hilbert spectral analysis

171 After having extracted the IMF modes, one can ap-
 172 ply the associated Hilbert spectral analysis to each com-
 173 ponent C_i in order to extract the energy time-frequency
 174 information from the data [38, 39, 60]. The Hilbert trans-
 175 form of a function $C(t)$ is written as

$$\tilde{C}(t) = \frac{1}{\pi} P \int \frac{C(t')}{t - t'} dt' \quad (9)$$

176 where P means the Cauchy principle value [37, 38, 60,
 177 61]. For each mode function $C_i(t)$, one can then construct
 178 the analytical signal [37, 61], $\mathbb{C}_i(t)$, as

$$\mathbb{C}_i(t) = C_i(t) + j\tilde{C}_i(t) = \mathcal{A}_i(t)e^{j\theta_i(t)} \quad (10)$$

179 where

$$\begin{cases} \mathcal{A}_i(t) = [C_i(t)^2 + \tilde{C}_i^2(t)]^{1/2} \\ \theta_i(t) = \arctan\left(\frac{\tilde{C}_i(t)}{C_i(t)}\right) \end{cases} \quad (11)$$

Hence the instantaneous frequency is defined as

$$\omega_i = \frac{1}{2\pi} \frac{d\theta_i(t)}{dt} \quad (12)$$

181 The original signal is finally represented [excluding the
 182 residual $r_n(t)$] as

$$x(t) = \mathbb{R} \sum_{i=1}^N \mathcal{A}_i(t)e^{j\theta_i(t)} = \mathbb{R} \sum_{i=1}^N \mathcal{A}_i(t)e^{j \int \omega_i(t) dt} \quad (13)$$

183 where "R" means real part. The above procedure is the
 184 classical Hilbert spectral analysis [37, 61]. The combina-
 185 tion of EMD and HSA is thus called Hilbert-Huang trans-
 186 form by some authors [43]. The Hilbert-Huang transform
 187 can be taken as a generalization of the Fourier trans-
 188 form, since it allows frequency modulation and ampli-
 189 tude modulation simultaneously. The Hilbert spectrum,
 190 $H(\omega, t) = \mathcal{A}^2(\omega, t)$, is designed to represent the energy
 191 in a time-frequency representation [60]. We further can
 192 define the Hilbert marginal spectrum as

$$h(\omega) = \int_0^{+\infty} H(\omega, t) dt \quad (14)$$

193 This is similar with the Fourier spectrum, and can be
 194 interpreted as the energy associated with each frequency.
 195 However, we underline the fact that the definition of fre-
 196 quency here is different from the definition in the Fourier
 197 frame. Thus the interpretation of the Hilbert marginal
 198 spectrum should be given more caution [38, 39].

199 3. Arbitrary-order Hilbert spectral analysis

200 We can also define the joint pdf $p(\omega, \mathcal{A})$ of the instanta-
 201 neous frequency ω and the amplitude \mathcal{A} for each of these
 202 IMF modes [31–33, 60]. The Hilbert marginal spectrum
 203 Eq. (14) is then rewritten as

$$h(\omega) = \int_0^{+\infty} p(\omega, \mathcal{A}) \mathcal{A}^2 d\mathcal{A} \quad (15)$$

204 The above definition is no more than the second-order
 205 statistical moment. This constatation has led some of
 206 us to recently generalize this approach to arbitrary-order
 207 moment $q \geq 0$ [31–33]

$$\mathcal{L}_q(\omega) = \int_0^{+\infty} p(\omega, \mathcal{A}) \mathcal{A}^q d\mathcal{A} \quad (16)$$

208 In case of scale invariance, we have

$$\mathcal{L}_q(\omega) \sim \omega^{-\xi(q)} \quad (17)$$

209 in which $\xi(q)$ is the Hilbert-based scaling exponent func-
 210 tion. Due to the integration operator, $\xi(q) - 1$ can be
 211 associated with $\zeta(q)$ from SF analysis [31, 33].

212 A limitation of the Hilbert-based method we proposed
 213 here is that it lacks the ability to consider $q < 0$ [62]. In

214 other words, similarly with the SF analysis, it has no res-
 215 olution on the right part of the singularity spectrum. The
 216 main drawback of the Hilbert-based method is its absence
 217 of solid theoretical ground, since the EMD part is almost
 218 empirical [43]. It has been found experimentally that
 219 the method, especially for the HSA, is statistically stable
 220 with different stopping criteria [42]. Recently, Flandrin
 221 et al. have obtained new theoretical results on the EMD
 222 method [41, 59, 63–65]. However, more theoretical work
 223 is still needed to fully mathematically understand this
 224 method.

225 B. Structure function analysis

226 The conventional way to extract scaling exponents is
 227 the classical SF analysis, which has been proposed in the
 228 field of turbulence and is now quite classical for intermit-
 229 tency studies [13]. The q th order SF is written as

$$S_q(\ell) = \langle |\Delta x_\ell(t)|^q \rangle \sim \ell^{\zeta(q)} \quad (18)$$

230 where $\Delta x_\ell(t) = x(t + \ell) - x(t)$ and ℓ is the time sepa-
 231 ration. The scaling exponent $\zeta(q)$ characterizes the fluc-
 232 tuation statistic at all scales; it is linear for monofractal
 233 processes such as fractional Brownian motion, and non-
 234 linear and concave (as a second Laplace characteristic
 235 function) for multifractal processes [66]. This approach
 236 has been widely used in turbulent research [1, 2, 13] and
 237 also other research fields [9, 67, 68]. However, the incre-
 238 ment operation acts a filter and thus SF characterizes the
 239 scale-invariant properties in an indirect way; see detailed
 240 discussion in Refs. [33, 36].

241 As we have shown elsewhere, the increment operation
 242 in SF acts a filter and is a global operation. It thus
 243 measures the scale invariant property in an indirect way.
 244 It is also found that it is strongly influenced by energetic
 245 large scale structures [33, 36]. Therefore the SF analysis
 246 is not suitable for those data which possess energetic large
 247 scale structures. We will show an example of passive
 248 scalar turbulence data with strong ramp-cliff structures
 249 in Sec. V. More discussion can be found in Refs. [33, 36].

250 C. Multifractal detrended fluctuation analysis

251 DFA was first introduced by Peng et al. [14] to study
 252 the scaling properties of DNA sequence, in which only
 253 the second-order moment $q = 2$ was considered. Later
 254 this was generalized into a multifractal version by con-
 255 sidering the arbitrary order q , namely multifractal de-
 256 trended fluctuation analysis (MFDFA) [17, 69]. It then
 257 became a more common technique for scaling data anal-
 258 ysis [14–17, 69–75]. For a given discrete time series $x(i)$,
 259 $i = 1 \cdots N$, we first estimate its cumulative function

$$Y(j) = \sum_{i=1}^j (x(i) - \bar{x}), \quad j = 1, \cdots, N \quad (19)$$

260 where \bar{x} is the mean value of x . We then divide it into
 261 M_n segments of length n ($n < N$) starting from both the
 262 beginning and the end of the time series. Each segment
 263 v has its own local trend that can be approximated by
 264 fitting a p th-order polynomial P_v^p which is removed from
 265 the data. The variances for all the segments v and for all
 266 segment lengths n are then calculated by

$$F^2(v, n) = \frac{1}{n} \sum_{j=1}^n \{Y[(v-1)n+j] - P_v^p(j)\}^2 \quad (20)$$

267 The q th-order fluctuation function is then defined as

$$F^q(n) = \left(\frac{1}{2M_n} \sum_{v=1}^{2M_n} [F^2(v, n)]^{q/2} \right)^{1/q} \quad (21)$$

268 For discussion convenience, we redefine the q th-order
 269 fluctuation function as

$$\mathcal{F}_q(n) = F^q(n)^q \quad (22)$$

270 In case of scale invariance, we have power law scaling
 271 within a significant range of n

$$\mathcal{F}_q(n) \sim n^{h(q)} \quad (23)$$

272 in which $h(q)$ is the corresponding scaling exponent func-
 273 tion.

274 D. Discrete wavelet transform and wavelet leaders

275 Wavelets have been widely used in data analysis
 276 and turbulence research [18–23, 25–27, 76–78]. Several
 277 wavelet-based methods have been proposed by several
 278 researchers to extract the scaling exponents from a scal-
 279 ing time series, for example, wavelet coefficients (WC),
 280 WTMM [18, 19, 76], WL [25, 26, 78], etc. We consider
 281 here WC and WL.

282 The discrete wavelet transform (DWT) is defined as

$$\psi(k, j) = \int_{\mathbb{R}} x(t) \varphi(2^{-j}t - k) dt \quad (24)$$

283 where φ is the chosen wavelet, $\psi(k, j)$ is the wavelet co-
 284 efficient, k is the position index, j is the scale index, and
 285 $\ell = 2^j$ is the corresponding scale [77, 79]. The first way
 286 to detect the scale-invariant properties is to consider the
 287 wavelet coefficients

$$Z_q(j) = \langle |\psi(k, j)|^q \rangle \sim 2^{j\tau(q)} \quad (25)$$

288 where $\tau(q)$ are the corresponding scaling exponents.

289 Every discrete wavelet coefficient $\psi(k, j)$ can be asso-
 290 ciated with the dyadic interval $\varrho(k, j)$

$$\varrho(k, j) = [2^j k, 2^j(k+1)) \quad (26)$$

291 Thus the wavelet coefficients can be represented as
 292 $\psi(\varrho) = \psi(k, j)$. Wavelet leaders are defined as

$$l(k, j) = \sup_{\varrho' \subset 3\varrho(k, j), j' \leq j} |\psi(\varrho')| \quad (27)$$

293 where $3\varrho(k, j) = \varrho(k-1, j) \cup \varrho(k, j) \cup \varrho(k+1, j)$ [25, 28, 78].
 294 Thus power law behavior is expected

$$\mathbb{Z}_q(j) = \langle l(k, j)^q \rangle \sim 2^{j\tau(q)} \quad (28)$$

295 in which $\tau(q)$ is the corresponding scaling exponent. Its
 296 efficiency has been shown for various types of data set
 297 [25–28, 78].

298 Let us recall some previous comparison studies be-
 299 tween WTMM, MF DFA and WL. Oświęcimka et al.
 300 [69] performed a comparison study between WTMM and
 301 MF DFA by analyzing synthesized data. They stated that
 302 the MF DFA provides a better estimation of singularity
 303 spectrum than WTMM. Jaffard et al. [25] stated that WL
 304 provides a better singularity spectrum than WTMM. Ser-
 305 rano and Figliola [27] performed a comparison study be-
 306 tween MF DFA and WL. They found that WL performs
 307 better than MF DFA. However, for a short time series,
 308 MF DFA is proposed to extract multifractal spectrum. A
 309 detailed comparison can be found in Ref. [25], [69], [27],
 310 respectively, for WTMM and WL, MF DFA and WTMM,
 311 and WL and MF DFA.

312 However, we argue here that DWT violates two facts of
 313 the time-frequency representation of a time series. First,
 314 the scale of a time series from complex system, for exam-
 315 ple, turbulent flows, is continuous in a statistical sense,
 316 but not discrete on several scales [31, 33]. The other one
 317 is that for a certain scale, it may not exist all the time
 318 [33, 38, 61]; see also the discussion in the next section.
 319 Thus to represent a signal by using a DWT is not con-
 320 sistent with the physical aspect.

321 III. NONLINEAR EFFECTS

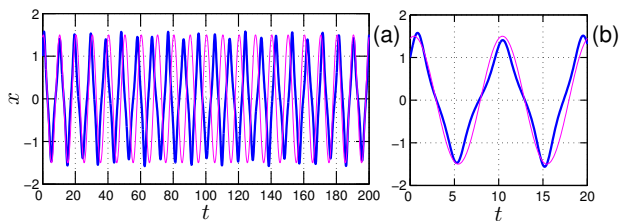


FIG. 1. (Color online) (a) a fifth order numerical solution (thick solid line) for Duffing equation, (b) An enlarged portion. For comparison, a sine wave with the same mean frequency is also shown as a thin solid line. The departure from a pure sine wave profile is the result of nonlinear interactions, which are nonlinear distortion.

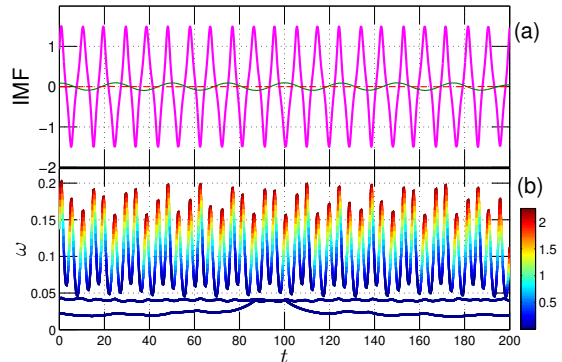


FIG. 2. (Color online) (a) The first three IMF modes from EMD; (b) the corresponding instantaneous frequency ω from Hilbert spectral analysis. Note the variation of the instantaneous frequency within one period. It is an intrawave-frequency-modulation, which corresponds to a nonlinear interaction. The instantaneous energy is encoded as a color.

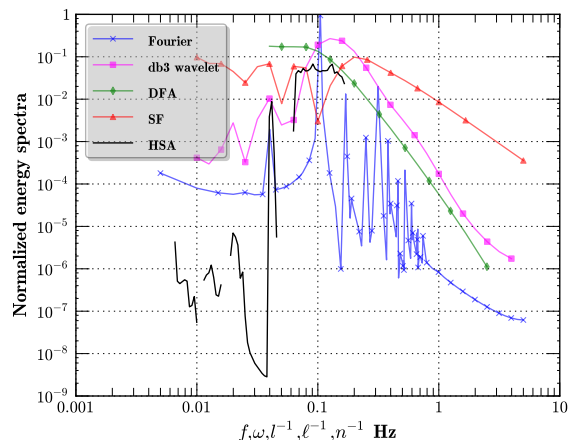


FIG. 3. (Color online) Energy spectra (the second-order statistical moments) provided by various methods: Fourier analysis (\times), continuous wavelet transform with db3 wavelet (\square), first-order DFA (\diamond), SF (\triangle) and Hilbert spectral analysis (solid line). The wavelet, SF and DFA spectra have been converted into spectral space by taking $f = 1/l$, $f = 1/\ell$ and $f = 1/n$, respectively. Except for the Hilbert-based method, all methods require high order harmonic components, which are not present in the original signal, see Figs. 1 and 2, to represent this nonlinear process. The high-order harmonics may lead to an artificial energy flux from low frequencies (large scales) to high frequencies (small scales) in spectral space.

322 We first consider nonlinear effects by using the classical
 323 Duffing equation, which reads

$$\frac{d^2x}{dt^2} + x(1 + \epsilon x^2) = b \cos(\Omega t) \quad (29)$$

324 in which ϵ is a nonlinear parameter. It can be consid-
 325 ered as a pendulum with forcing function $b \cos(\Omega t)$, in
 326 which its pendulum length varies with the angle. Fig-
 327 ure 1 shows a fifth-order Runge-Kutta numerical solu-

tion (thick solid line) with $\epsilon = 1$, $b = 0.1$, $\Omega = 2\pi/25$, and $[x(0), x'(0)] = [1, 1]$. The sampling frequency sets as 10 Hz. For comparison, we also show a pure sine wave (thin solid line) with the same mean frequency. One can see that the wave profile of the solution of the Duffing equation is significantly deviating from a sine wave. This deviation is the result of nonlinear interaction, namely nonlinear distortion [38, 39]. It is also clearly shown that there are no high-order harmonic components in the physical domain [33]. Figure 2 shows the first three IMF modes obtained from EMD decomposition and the corresponding instantaneous frequency ω from Hilbert spectral analysis. The instantaneous energy is encoded as a color. The instantaneous frequency ω of the first IMF mode is varying within one period. This corresponds to the so-called intrawave-frequency-modulation, which is associated with the nonlinear interactions [33, 38, 39]. It also clear shows that for a certain frequency, it may not exist clearly all the time.

Figure 3 shows the normalized energy spectra (or the second-order statistical moments) provided by various methods: Fourier analysis (\times), continuous wavelet transform with db3 wavelet (\square), the first-order DFA (\diamond), SF (\triangle) and HSA (solid line). For display convenience, the wavelet, DFA and SF spectra have been converted from physical domain into frequency domain by taking $f = 1/l$, $f = 1/n$ and $f = 1/\ell$, respectively. We emphasize here that different wavelet families provide a similar spectral curve (not shown here). As pointed out by Huang et al. [38] wavelet transform can be considered as an adjustable window Fourier transform. Thus it inherits the shortcomings of the Fourier transform. We observe that except for the Hilbert spectral analysis, all methods require high-order harmonic components to represent this nonlinear process. High-order harmonic components are not present in the time series (see Figs. 1 and 2). It is thus a requirement of the method itself, not the physics [33, 38]. This is the main drawback of traditional methods, in which the basis is given *a priori*. Therefore it is inevitable that one requires high-order harmonic components to represent the difference between the analyzed signal and the given basis. We argue here that high order harmonic components may lead to an artificial energy flux from low frequencies (large scales) to high frequencies (small scales) in spectral space. Therefore, power law behavior, if it exists, may be contaminated by this artificial energy flux. We will show this point experimentally by analyzing a temperature data set with strong ramp-cliff structures in Sec. V.

IV. VALIDATION AND CALIBRATION

In this section, we will validate the Hilbert-based method by performing a comparison study of simulated fBm with Hurst number $H = 1/3$ and synthesized multifractal random walk with an intermittent parameter $\mu = 0.15$. For comparison convenience, spectral curves (or the

q th-order statistical moment) provided by SFs, MFDFA and wavelet are converted from the physical domain into the spectral domain by taking $f = 1/\ell$, $f = 1/n$, and $f = 1/l$, respectively. The corresponding scaling exponents are estimated on the range $0.001 < f < 0.1$ (we set here the sampling frequency as 1). Wavelet transform is performed by using the db3 wavelet. Due to the limitation of the SF analysis and the HSA, we only consider here the non-negative q th-order moment, $q \geq 0$, the left part of the singularity spectrum.

A. Fractional Brownian motion

We have shown in previous works that the arbitrary-order HSA can be applied to the fractional Brownian motion [31, 32]. Here we briefly recall these results. fBm is a Gaussian self-similar process with a normal distribution increment, which is characterized by H , the Hurst number $0 < H < 1$ [80–83]. Note that the singularity spectra for the above mentioned methods are

$$\alpha = \zeta'(q), \quad f(\alpha) = \min_q \{\alpha q - \zeta(q) + 1\} \quad (30a)$$

for SFs, and

$$\alpha = \xi'(q), \quad f(\alpha) = \min_q \{\alpha q - \xi(q) + 2\} \quad (30b)$$

for the Hilbert-based method, and

$$\alpha = h'(q) - 1, \quad f(\alpha) = \min_q \{(\alpha + 1)q - h(q) + 1\} \quad (30c)$$

for DFA, and

$$\alpha = \tau'(q) - 1, \quad f(\alpha) = \min_q \{(\alpha + 1)q - \tau(q) + 1\} \quad (30d)$$

for WC and WL, respectively. Ideally, we should have $\alpha = H$ and $f(\alpha) = 1$.

We performed 500 realizations each of length 2^{14} data points by applying a Fourier-based Wood-Chan algorithm [84] with $H = 1/3$, which corresponds to the Hurst number of turbulent velocity. We apply the above mentioned methods to each realization of the data series. The final spectra and statistical errors are then estimated from these 500 realizations. Figure 4 show results for (a) SF: (left) $S_q(\ell)$ with $q = 0$ (\circ), $q = 2$ (\square), $q = 4$ (\triangle) and $q = 6$ (∇), (middle) the corresponding scaling exponents $\zeta(q)$ on the range $0 \leq q \leq 8$, (right) the corresponding singularity spectrum $f(\alpha)$, (b) HSA, (c) DFA, and (d) wavelet, respectively. The symbols are the same as the SF symbols. Graphically, all methods provide comparable estimation of $f(\alpha)$. However, we note that the Hilbert-based method slightly overestimates $\xi(q)$ when $q > 6$. Additionally both the first- and second-order DFA provide slight underestimation of $h(q)$ and seem to predict a systematic underestimation of the Hurst number H . The WC and WL provide almost the same estimation

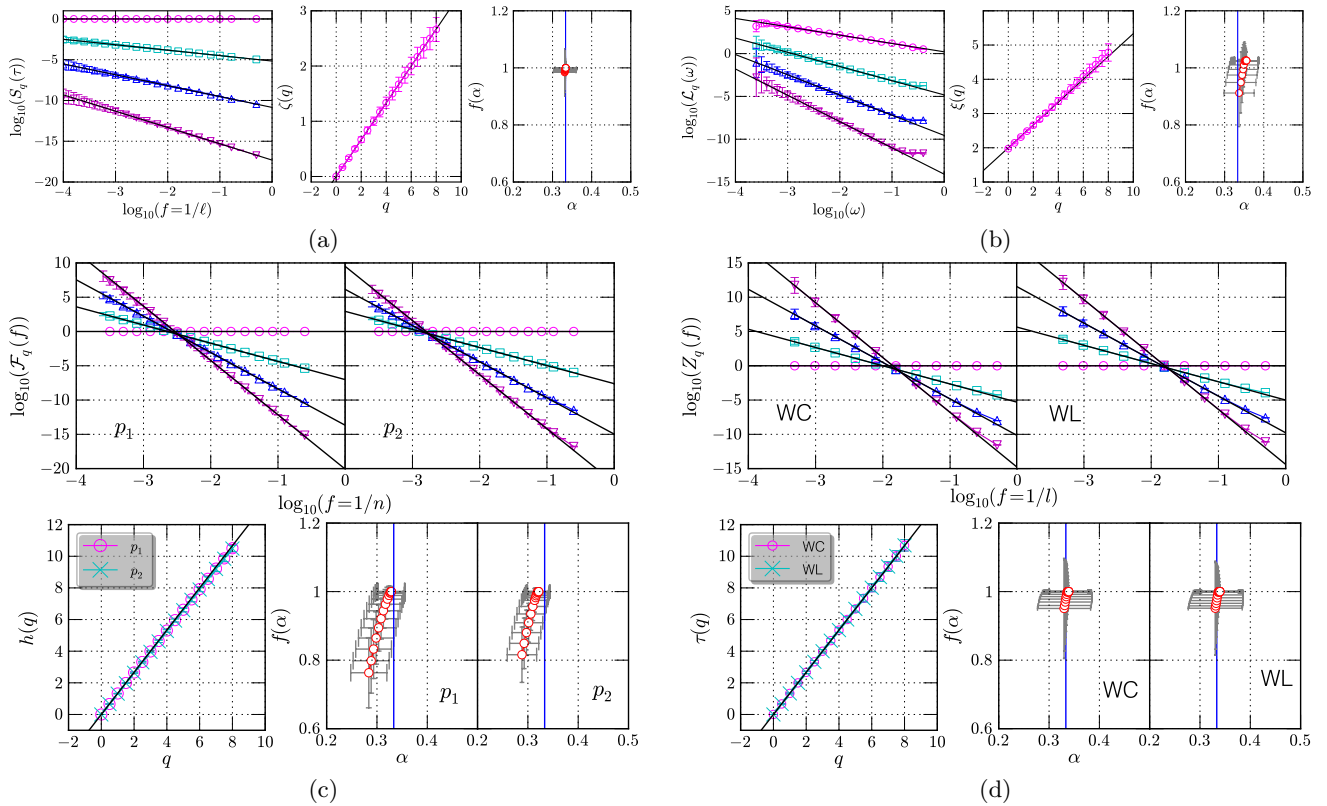


FIG. 4. (Color online) Analysis results of fBm with Hurst number $H = 1/3$. (a) structure functions. left: $S_q(\ell)$ with $q = 0$ (\circ), $q = 2$ (\square), $q = 4$ (\triangle) and $q = 6$ (∇); middle: the corresponding scaling exponents $\zeta(q)$ on the range $0 \leq q \leq 8$; right: the corresponding singularity spectrum $h(\alpha)$. (b) results of Hilbert spectral analysis. (c) multifractal detrended fluctuation analysis (d) wavelet coefficients and wavelet leaders. The symbols are the same as for structure functions. Scaling exponents are estimated in the range $-3 < \log_{10}(f) < -1$. The statistical errors are estimated from a total of 500 realizations.

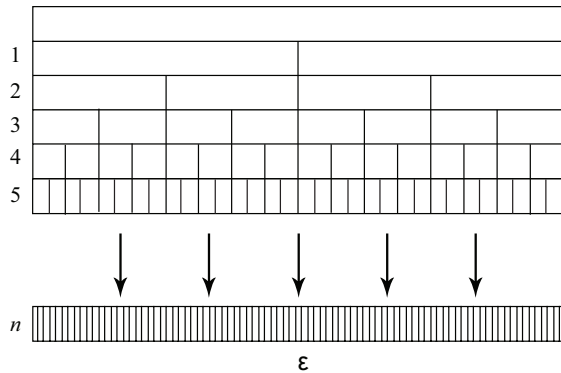


FIG. 5. Illustration of the discrete cascade process. Each step is associated with a scale ratio of 2. After n steps, the total scale ratio is 2^n .

425 for this simple monofractal process. It seems that they
 426 provide a better estimation than Hilbert and DFA meth-
 427 ods. This result is not in full agreement with Oświęcimka
 428 et al. [69], who stated that the MF DFA provides a better
 429 estimation of H than WTMM.

430 The above results show that all methods provide com-
 431 parable prediction of singularity spectra for fBm with

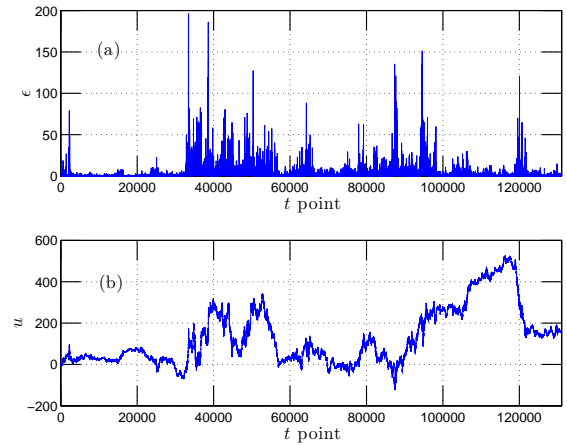


FIG. 6. A sample for one realization of length 2^{17} points with $\mu = 0.15$, (a) the multifractal measure, and (b) the constructed multifractal nonstationary process.

432 $H = 1/3$. However, it seems that SF and wavelet based
 433 methods provide a better estimation.

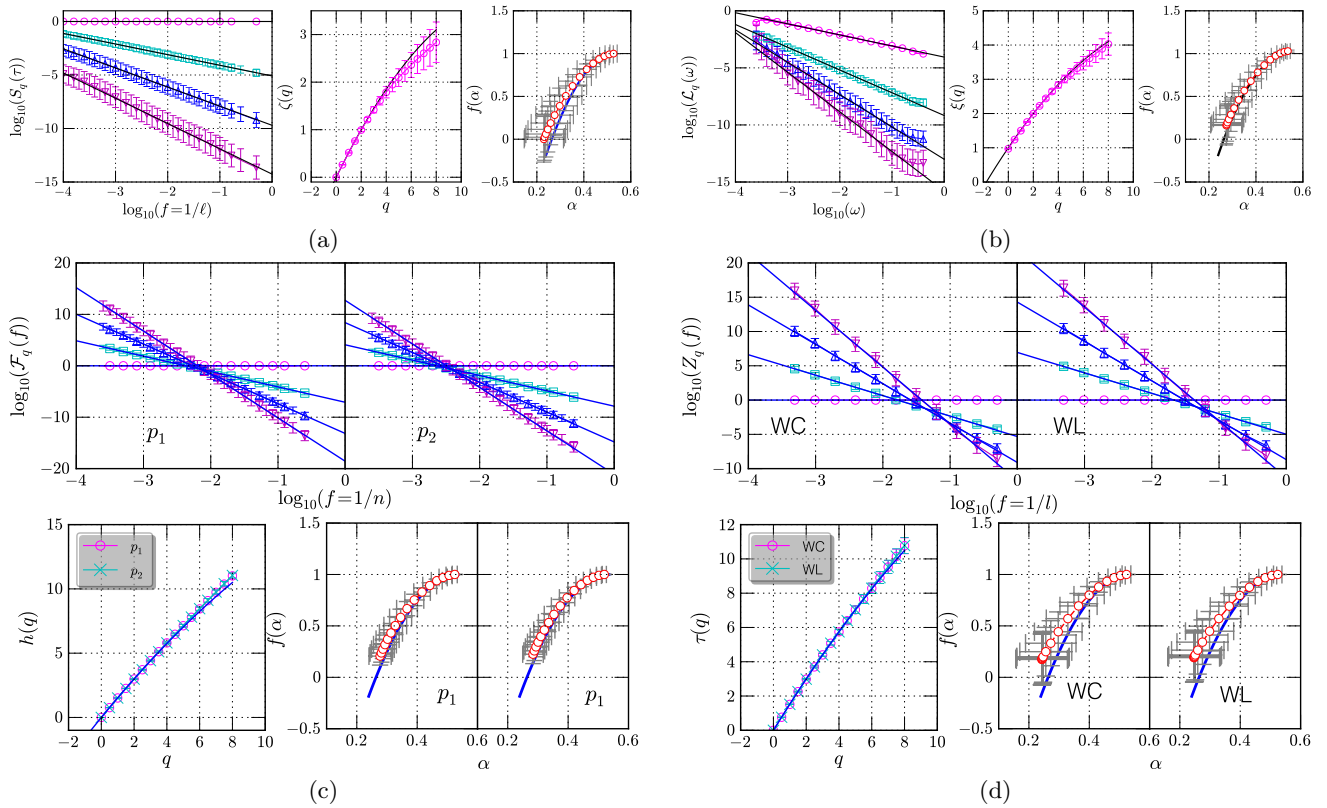


FIG. 7. (Color online) Multifractal random walk with $\mu = 0.15$. (a) Structure function, (b) Hilbert spectral analysis, (c) multifractal detrended fluctuation analysis and (d) wavelet coefficients and wavelet leaders. The symbols are the same as in Fig. 4. The statistical error bars are estimated from the total 100 realizations.

B. Multifractal simulation

We show now that the new method applies to multifractal time series. First, let us consider a multiplicative discrete cascade process to simulate a multifractal measure $\epsilon(x)$. Figure 5 illustrates the cascade process algorithm. The larger scale corresponds to a unique cell of size $L = \ell_0 \lambda_1^n$, where ℓ_0 is a fixed scale and $\lambda_1 > 1$ is a dimensional scale ratio. For discrete models, this ratio is often taken as $\lambda_1 = 2$. The models being discrete, the next scale involved corresponds to λ_1 cells, each of size $L/\lambda_1 = \ell_0 \lambda_1^{n-1}$. This is iterated and at step p ($1 \leq p \leq n$) there are λ_1^p cells, each of size $L/\lambda_1^p = \ell_0 \lambda_1^{n-p}$. There are n cascade steps, and at step n there are λ_1^n cells, each of size ℓ_0 , which is the smallest scale of the cascade. To reach this scale, all intermediate scales have been involved. Finally, at each point the multifractal measure writes as the product of n cascade random variables

$$\epsilon(x) = \prod_{p=1}^n W_{p,x} \quad (31)$$

where $W_{p,x}$ is the random variable corresponding to position x and level p in the cascade [85]. Following multifractal random walk ideas [86, 87], we generate a non-

stationary multifractal time series as

$$u(x) = \int_0^x \epsilon(x')^{1/2} dB(x') \quad (32)$$

where $B(x)$ is Brownian motion. Taking lognormal statistic for ϵ , the scaling exponent $\zeta(q)$ such as $\langle |\Delta u_\tau(t)|^q \rangle \sim \tau^{\zeta(q)}$ can be shown to be written as

$$\zeta(q) = \frac{q}{2} - \frac{\mu}{2} \left(\frac{q^2}{4} - \frac{q}{2} \right) \quad (33)$$

where μ is the intermittency parameter ($0 \leq \mu \leq 1$) characterizing the lognormal multifractal cascade.

Synthetic multifractal time series are generated following Eq. (32). For each realization, we choose $n = 17$ levels, corresponding to data sets with data length 131,072 points each. A sample for one realization is shown in Fig. 6 (a) for the multifractal measure and (b) for the nonstationary multifractal time series with $\mu = 0.15$. We perform 100 realizations with intermittent parameter $\mu = 0.15$. Except for the structure functions, we apply all methods to each realization by dividing one realization into eight subsets with 2^{14} data points each. The spectra for each realization are averaged over these eight subsets. The final spectra and error bars are respectively ensemble average and standard deviation estimated from these 100 realizations.

475 Figure 7 shows the results of (a) SF, (b) HSA, (c)
 476 MFDEFA and (d) WC and WL, respectively. The sym-
 477 bols are the same as in Fig. 4. The theoretical scaling
 478 exponents and the corresponding singularity spectrum
 479 $f(\alpha)$ on the range $0 < q < 8$ are shown as a solid line in
 480 the corresponding sub figures. We see that SFs under-
 481 estimate $\zeta(q)$ when $q > 4$. The corresponding estimated
 482 singularity spectrum $f(\alpha)$ deviates from the theoretical
 483 line when $\alpha < 0.4$, corresponding to $q > 2.5$. It also has
 484 the largest statistical error. Hilbert methodology slightly
 485 underestimates $\xi(q)$ when $q > 5$. It provides a better esti-
 486 mation of scaling exponents and $f(\alpha)$ than SFs. MFDEFA
 487 provides the smallest statistical errors for spectral curves
 488 $\mathcal{F}_q(n)$, scaling exponents $h(q)$ and singularity spectrum
 489 $f(\alpha)$. However, it still slightly overestimates $h(q)$ when
 490 $q > 6$. We note that the first- and second-order DFA
 491 provide an equivalent result. WC and WL predict al-
 492 most the same spectral curves, scaling exponents $\tau(q)$
 493 and singularity spectrum $f(\alpha)$. The corresponding sin-
 494 gularity spectrum significantly deviates from the theo-
 495 retical curve. We also note that none of these methods
 496 recover the whole theoretical line on the range $0 < q < 8$.

497 V. PASSIVE SCALAR TURBULENCE WITH 498 RAMP-CLIFF STRUCTURES

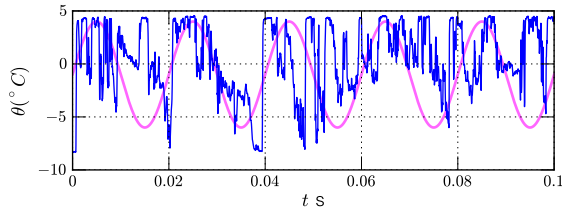


FIG. 8. (Color online) A 0.1 s portion of temperature data showing strong ramp-cliff structures. For comparison, a pure sine wave is also shown as a thick solid line. Note that the ramp-cliff structure is significantly different from a sine wave, which may cause serious artificial energy flux in Fourier spectral space.

499 We now apply the above-mentioned methods to a real
 500 time data set, a temperature time series as a turbulent
 501 passive scalar. The data are obtained from a jet experi-
 502 ment performed at Joseph Fourier University Grenoble,
 503 France. The bulk Reynolds number is about $Re \simeq 60000$.
 504 The corresponding Taylor's microscale Reynolds number
 505 is about $Re_\lambda \simeq 250$. The initial temperature of the two
 506 flows are $T_J = 27.8^\circ\text{C}$ and $T = 14.8^\circ\text{C}$. The measure-
 507 ment location is in the mixing layer and close to the noz-
 508 zle of the jet. The sampling frequency is 50 kHz. The
 509 total data length is 10 s, corresponding to 500,000 data
 510 points. Figure 8 shows a 0.1 s portion temperature data,
 511 illustrating strong ramp-cliff structures. For comparison,
 512 a pure sine wave is also shown. Obviously, the so-called
 513 ramp-cliff structure is a large-scale structure with a very
 514 sharp interface [88–91]. We note that the profile of ramp-

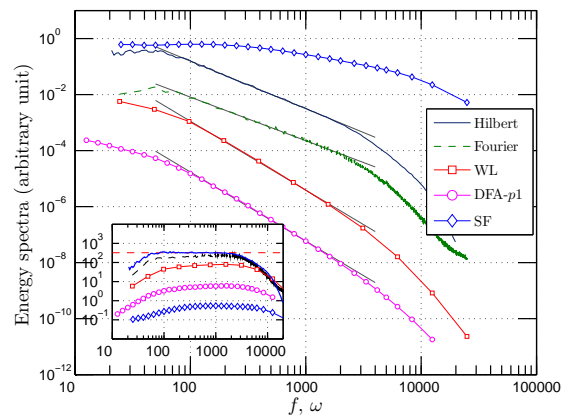


FIG. 9. (Color online) Energy spectra (or the second-order statistical moment) provided by several methods. The inset shows the compensated spectra by multiplying the result by $f^{5/3}$ for Hilbert and Fourier, $f^{8/3}$ for DFA and wavelet, and $f^{2/3}$ for SFs, respectively. For clarity, the curves have been vertically shifted. Both Fourier and Hilbert methods predict a clear power law on the range $80 < \omega < 2000$ Hz. Due to the presence of ramp-cliff structures, the SF analysis fails to capture the power law behavior and DFA and wavelet predict a short inertial range on the range $100 < f < 1000$ Hz. The corresponding scaling exponents are $\beta_\theta = 1.56$ for Fourier, $\xi_\theta(2) = 1.70$ for Hilbert, $\tau_\theta(2) = 2.46$ for WL with db3 wavelet, and $h_\theta(2) = 2.47$ for the first-order DFA, respectively.

515 cliff structures is significantly deviating from a sine wave.
 516 Thus for the Fourier-based methodologies, it is inevitable
 517 that one requires high-order harmonic components to
 518 represent their difference, in which the underlying idea
 519 is a linear asymptotic approximation [37, 38, 61]. This
 520 linear asymptotic approximation process thus leads to an
 521 artificial energy flux from low frequencies (large scales)
 522 to higher frequencies (small scales). It means that the
 523 Fourier-based spectrum may be contaminated by this arti-
 524 ficial energy flux. As another direct consequence, the
 525 artificial redistribution of the energy will lead to an un-
 526 real correlation if we consider cross-correlation between
 527 two scales [92].

528 The original time series is divided into 122 non-
 529 overlapping segments with 2^{12} data points each. The
 530 finally spectra and statistical errors (the standard devi-
 531 ation) are then estimated from these 122 realizations.
 532 Figure 9 shows the energy spectra (or the second order
 533 statistical moments) provided by HSA (solid line),
 534 Fourier transform (dashed line), WL (\square), the first-order
 535 DFA (\circ) and SF (\diamond), respectively. The inset shows
 536 the corresponding compensated spectra by multiplying
 537 a Kolmogorov-Obukhov-Corrsin [93–95] nonintermittent
 538 scaling exponent $5/3$ for Hilbert spectrum, Fourier power
 539 spectrum, $8/3$ for WL and DFA, and $2/3$ for SF, respec-
 540 tively. Except for the SF, all methods display a clear
 541 power law on the range $80 < f < 2000$ Hz or $100 <$
 542 $f < 1000$ Hz, a more than one decade inertial range.
 543 The corresponding scaling exponents are $\xi_\theta(2) \simeq 1.70$

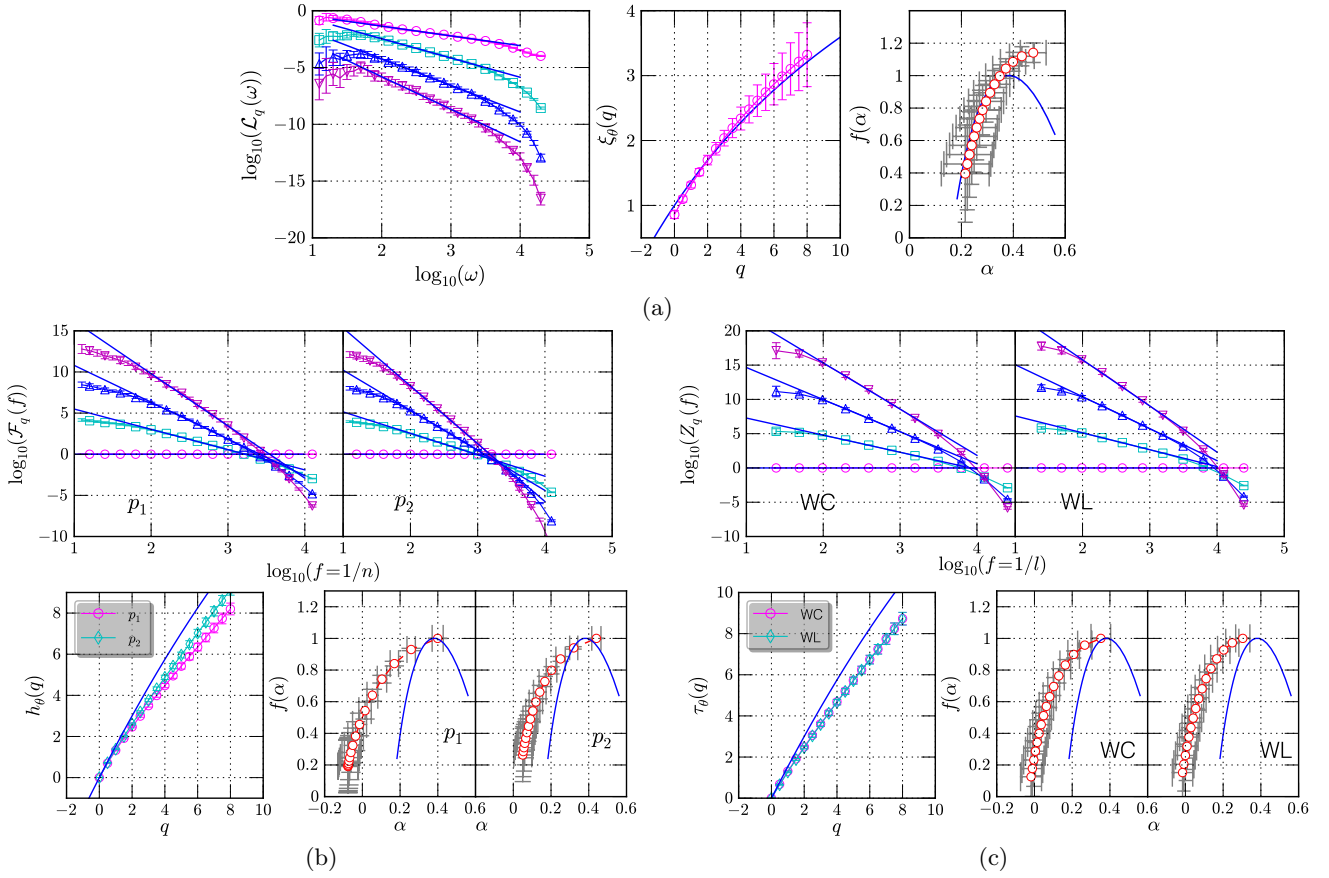


FIG. 10. (Color online) Results for passive scalar (temperature) with strong ramp-cliff (a) Hilbert spectral analysis, (b) multifractal detrended fluctuation analysis, and (c) wavelet coefficients and wavelet leaders. The symbols are the same as in Fig. 4.

544 for Hilbert, $\beta_\theta \simeq 1.56$ for Fourier, $\tau_\theta(2) \simeq 2.46$ for
 545 WL and $h_\theta(2) \simeq 2.47$ for DFA, respectively obtained
 546 by using a least square fitting algorithm. We note that
 547 only the Hilbert based scaling exponent $\xi_\theta(2)$ is close
 548 to the corresponding nonintermittent scaling exponent
 549 $\xi_\theta(2) = 5/3$ [36]. It is also comparable with the scaling
 550 exponent of longitudinal velocity in fully developed tur-
 551 bulance [2, 96, 97]. Due to the presence of strong ramp-
 552 cliff structures, the SF fails to detect the correct scaling
 553 behavior. The influence of large energetic structures on
 554 SF has been studied in detail by Huang et al. [36] and
 555 Huang [33]. It is interesting to note that DFA and WL
 556 provide almost the same scaling exponent, which indi-
 557 cates that the ramp-cliff structure may have the same
 558 influence on them. We believe that there exists an arti-
 559 ficial energy flux as we discussed above in both Fourier
 560 and DFA and WL spectra. Thus they may underestimate
 561 the scaling exponents [36].

562 Figure 10 shows the analysis results of (a) Hilbert spec-
 563 tral analysis, (b) MFDFA, and (c) wavelet transform,
 564 respectively. The symbols are the same as in Fig. 4.
 565 For comparison, the lognormal model of longitudinal ve-
 566 locity [98] is shown as a solid line in the subfigures of
 567 scaling exponents and singularity spectra. Due to the

568 failure of SF analysis, we do not present it here (see
 569 Ref. [33]). Graphically, these three methodologies pre-
 570 dict power law spectra with small statistical error. The
 571 corresponding scaling exponents are estimated on the
 572 range $80 < f < 2000$ Hz or $100 < f < 1000$ Hz. It
 573 is found that the corresponding scaling exponents $\xi_\theta(q)$
 574 and singularity spectrum $f(\alpha)$ are close to the lognor-
 575 mal fitting model, indicating a less intermittent passive
 576 scalar turbulence field than what was believed before [36].
 577 MFDFA and wavelets provide comparable statistical er-
 578 rors and singularity spectra. Their scaling exponents and
 579 singularity spectra significantly deviate from lognormal
 580 model, which is usually considered as evidence that the
 581 passive scalar turbulence field is much more intermittent
 582 than the velocity field [88–91]. We note that the first-
 583 and second-order MFDFA provide different scaling expo-
 584 nents and singularity spectra, which may be associated
 585 with the different abilities of different order polynomials
 586 [15, 71].

587 As we already mentioned previously, the wavelet and
 588 DFA spectra are strongly influenced by nonlinear large
 589 scale structures (e.g. ramp-cliff structures in passive
 590 scalar turbulence). Their scaling exponents are thus con-
 591 taminated by high-order harmonics. In other words, the

592 statistical property of small scales is contaminated by
 593 nonlinear large-scale structures. We believe here that
 594 the scaling exponents and singularity spectrum provided
 595 by them are not correct. Since the HSA has a very local
 596 ability in both physical and spectral spaces, together
 597 with the ability of intrawave-frequency-modulation for
 598 nonlinear processes, the effect of ramp-cliff structures is
 599 constrained in the amplitude-frequency space. Therefore,
 600 the HSA method may provide a more correct scaling ex-
 601 ponent and singularity spectrum. We note that for DFA
 602 and the wavelet method, the large deviation from a log-
 603 normal spectrum may be interpreted as a shift problem
 604 for moment-based methods when the translational invari-
 605 ance is broken [29, 30]. It seems that the Hilbert-based
 606 method can automatically correct this problem. We also
 607 underline here that the Reynolds number of the present
 608 passive scalar data set is about $Re_\lambda \simeq 250$. Thus the
 609 strong ramp-cliff structure may be recognized as an ef-
 610 fect of the finite Reynolds number. We will address this
 611 issue elsewhere.

612 VI. CONCLUSION

613 In summary, we introduced in this paper a new
 614 method, namely arbitrary-order Hilbert spectral anal-
 615 ysis, to characterize scale-invariant properties directly
 616 in the amplitude-frequency space [31–33]. It is an ex-
 617 tended version of Hilbert-Huang transform [38, 39, 43].
 618 The main advantage of the Hilbert-based methodology
 619 is its fully adaptive [41] and very local ability both in
 620 spectral and physical domains [38, 39]. Thus, it is not
 621 necessary to require high-order harmonics to represent
 622 nonlinear and nonstationary processes, which is usually
 623 required by conventional Fourier-based methods, such as
 624 Fourier transform, wavelet transform, etc. We illustrated
 625 the nonlinear effect by using the Duffing equation. It is
 626 found that not only Fourier-based methods, but also SF
 627 analysis and DFA are influenced by nonlinear processes.
 628 It is also found that the HSA can constrain the high-order
 629 harmonics by using the intrawave-frequency-modulation
 630 mechanism for the nonlinear distortion [38, 39, 43].

631 We then performed a comparison study of the Hilbert-
 632 based methodology with SF analysis, MFDFA, and WL,
 633 by analyzing fBm simulations with Hurst number $H =$
 634 $1/3$ and a synthesized multifractal lognormal random
 635 walk with intermittent parameter $\mu = 0.15$, respectively.
 636 For the former simulation, we considered the scaling ex-
 637 ponents and singularity spectrum on the range $0 < q < 8$.
 638 It was found that all methods provide comparable scaling
 639 exponents and singularity spectra. For the latter synthe-
 640 sized multifractal random walk data, HSA and MFDFA
 641 provide a better estimation of singularity spectra than
 642 SF and WL. However, none of these methods recover the
 643 whole spectrum. We finally applied all methods to the
 644 passive scalar (temperature) data set with strong ramp-
 645 cliff structure, which is an important signature of passive
 646 scalar turbulence [89, 90]. We found that except for HSA,

647 all the methods require high-order harmonics to represent
 648 the ramp-cliff structures. Therefore, the singularity spec-
 649 tra provided by DFA and WL are contaminated by this
 650 large nonlinear structure. In fact, it already has been
 651 reported by several authors that for passive scalar tur-
 652 bulence the second-order SF and Fourier power spectrum
 653 are not consistent with each other [90, 99, 100]. Warhaft
 654 [90] stated that “the reason for this is unclear, but appar-
 655 ently stems from the Fourier transform itself.” There is
 656 no mathematical transform involved in SF analysis. Now,
 657 it seems quite clear that not only Fourier-based methods
 658 are strongly influenced by the ramp-cliff structure, but
 659 also SF analysis [36] and DFA.

660 Our experience is that the HSA is a direct mea-
 661 surement of scale-invariant property in the amplitude-
 662 frequency space. It thus requires a much larger sample
 663 size to get a convergence result than SFs, DFA and WL.
 664 Thus for a sample of small size without large-scale struc-
 665 tures, SF analysis, DFA or WL are useful to extract scal-
 666 ing exponents and singularity spectrum since all method-
 667 ologies provide almost the same result. In this situation,
 668 the HSA is useful to catch the scaling trend. However,
 669 if the data set possesses a large-scale structure (e.g., the
 670 ramp-cliff structure in passive scalar turbulence, the sea-
 671 sonal cycle in the daily discharge of river flow, etc.), we
 672 argue that the HSA is the best choice.

673 Finally, we would like to provide some comments on
 674 the moment-based methods, for example, the methods
 675 presented in this work, and the singularity-based ap-
 676 proaches (e.g. GMWP [29, 30]). Due to the convergence
 677 problem, the moment-based methods seem to require a
 678 much larger sample size than the singularity-based ap-
 679 proaches. Thus the statistical error bars presented in
 680 this paper could be non-significant due to the finite sam-
 681 ple size. Another issue is the right part of the singular-
 682 ity spectrum, which corresponds to evaluating the neg-
 683 ative order statistical moments for the moment-based
 684 methods. As we already mentioned previously, it may
 685 be inaccessible for most of the moment-based methods
 686 [30]. However, the singularity-based methods can over-
 687 come this problem [29, 30]. It seems that the idea of the
 688 singularity-based approaches can be extended into the
 689 Hilbert frame. This will be presented in a future work.

690 ACKNOWLEDGMENTS

691 This work is supported in part by the National Natu-
 692 ral Science Foundation of China (Grant No.10772110 and
 693 No. 11072139) and the Shanghai Program for Innovative
 694 Research Team in Universities. Y. H. was financed in
 695 part by a grant from the French Ministry of Foreign Af-
 696 fairs and in part by Université Lille. Y.H. also acknowl-
 697 edges a financial support from EHL of Université Libre de
 698 Bruxelles during the preparation of this manuscript. We
 699 thank Professor P. Abry from Laboratoire de Physique,
 700 CNRS and ENS Lyon (France) for providing his wavelet
 701 leader codes. The EMD Matlab codes used in this paper

- are written by Dr. Gabriel Rilling and Professor Patrick Flandrin from Laboratoire de Physique, CNRS and ENS Lyon (France): [10].
-
- [1] F. Anselmet, Y. Gagne, E. J. Hopfinger, and R. A. Antonia, *J. Fluid Mech.* **140**, 63 (1984).
- [2] U. Frisch, *Turbulence: the legacy of AN Kolmogorov* (Cambridge University Press, 1995).
- [3] D. Lohse and K.-Q. Xia, *Ann. Rev. Fluid Mech.* **42**, 335 (2010).
- [4] D. Schertzer and S. Lovejoy, *J. Geophys. Res.* **92**, 9693 (1987).
- [5] F. G. Schmitt, S. Vannitsem, and A. Barbosa, *J. Geophys. Res.* **103**, 23181 (1998).
- [6] M. De Lima and J. Grasman, *J. Hydrol.* **220**, 1 (1999).
- [7] V. Venugopal, S. G. Roux, E. Foufoula-Georgiou, and A. Arneodo, *Phys. Lett. A* **348**, 335 (2006).
- [8] S. Ghashghaie and Y. Dodge, *Nature* **381**, 27 (1996).
- [9] F. G. Schmitt, D. Schertzer, and S. Lovejoy, *Appl. Stoch. Models and Data Anal.* **15**, 29 (1999).
- [10] T. Lux, *Quantitative Finance* **1**, 560 (2001).
- [11] L. Calvet and A. Fisher, *Review of Economics and Statistics* **84**, 381 (2002).
- [12] P. Ivanov, A. Bunde, L. Amaral, S. Havlin, J. Fritsch-Yelle, R. Baevsky, H. Stanley, and A. Goldberger, *Europhys. Lett.* **48**, 594 (1999).
- [13] A. S. Monin and A. M. Yaglom, *Statistical fluid mechanics vd II* (MIT Press Cambridge, Mass, 1971).
- [14] C.K. Peng, S.V. Buldyrev, S. Havlin, M. Simons, H.E. Stanley, and A.L. Goldberger, *Phys. Rev. E* **49**, 1685 (1994).
- [15] K. Hu, P.C. Ivanov, Z. Chen, P. Carpena, and H.E. Eugene Stanley, *Phys. Rev. E* **64**, 11114 (2001).
- [16] A. Bashan, R. Bartsch, J. Kantelhardt, and S. Havlin, *Physica A* **387**, 5080 (2008).
- [17] J. Kantelhardt, S. Zschiegner, E. Koscielny-Bunde, S. Havlin, A. Bunde, and H. Stanley, *Physica A* **316**, 87 (2002).
- [18] J.F. Muzy, E. Bacry, and A. Arneodo, *Phys. Rev. Lett.* **67**, 3515 (1991).
- [19] J.F. Muzy, E. Bacry, and A. Arneodo, *Phys. Rev. E* **47**, 875 (1993).
- [20] J. Arrault, A. Arneodo, A. Davis, and A. Marshak, *Phys. Rev. Lett.* **79**, 75 (1997).
- [21] C. Rodrigues Neto, A. Zanandrea, F. Ramos, R. Rosa, M. Bolzan, and L. Sá, *Physica A* **295**, 215 (2001).
- [22] M. Farge, N. Kevlahan, V. Perrier, and E. Goirand, *IEEE J PROC* **84**, 639 (1996).
- [23] M. Farge, *Annu. Rev. Fluid Mech.* **24**, 395 (1992).
- [24] J. Ghez and S. Vaienti, *J. Statist. Phys.* **57**, 415 (1989).
- [25] S. Jaffard, B. Lashermes, and P. Abry, *Wavelet Analysis and Applications* (2005).
- [26] B. Lashermes, S. Roux, P. Abry, and S. Jaffard, *EPJB* **61**, 201 (2008).
- [27] E. Serrano and A. Figliola, *Physica A* **388**, 2793 (2009).
- [28] B. Lashermes, S. Jaffard, and P. Abry, *ICASSP 2005*, Philadelphia, USA, (2005).
- [29] O. Pont, A. Turiel, and C. Pérez-Vicente, *Physical Review E* **74**, 061110 (2006).
- [30] A. Turiel, C.J. Pérez-Vicente, and J. Grazzini, *J. Comput. Phys.* **216**, 362 (2006).
- [31] Y. Huang, F. G. Schmitt, Z. Lu, and Y. Liu, *Europhys. Lett.* **84**, 40010 (2008).
- [32] Y. Huang, F. G. Schmitt, Z. Lu, and Y. Liu, *Traitement du Signal* **25**, 481 (2008).
- [33] Y. Huang, *Arbitrary Order Hilbert Spectral Analysis: Definition and Application to fully developed turbulence and environmental time series*, Ph.D. thesis, Université des Sciences et Technologies de Lille - Lille 1, France & Shanghai University, China (2009);<http://tel.archives-ouvertes.fr/tel-00439605/fr..>
- [34] F. G. Schmitt, Y. Huang, Z. Lu, L. Y., and N. Fernandez, *J. Mar. Sys.* **77**, 473 (2009).
- [35] Y. Huang, F. G. Schmitt, Z. Lu, and Y. Liu, *J. Hydrol.* **373**, 103 (2009).
- [36] Y. Huang, F. Schmitt, Z. Lu, P. Fougairolles, Y. Gagne, and Y. Liu, *Phys. Rev. E* **82**, 26319 (2010).
- [37] L. Cohen, *Time-frequency analysis* (Prentice Hall PTR Englewood Cliffs, NJ, 1995).
- [38] N. E. Huang, Z. Shen, S. R. Long, M. C. Wu, H. H. Shih, Q. Zheng, N. Yen, C. C. Tung, and H. H. Liu, *Proc. R. Soc. London, Ser. A* **454**, 903 (1998).
- [39] N. E. Huang, Z. Shen, and S. R. Long, *Annu. Rev. Fluid Mech.* **31**, 417 (1999).
- [40] G. Rilling, P. Flandrin, and P. Gonçalvès, *IEEE-EURASIP Workshop on Nonlinear Signal and Image Processing* (2003).
- [41] P. Flandrin and P. Gonçalvès, *Int. J. Wavelets, Multires. Info. Proc.* **2**, 477 (2004).
- [42] N. E. Huang, M. L. Wu, S. R. Long, S. S. P. Shen, W. Qu, P. Gloersen, and K. L. Fan, *Proc. R. Soc. London, Ser. A* **459**, 2317 (2003).
- [43] N. E. Huang, *Hilbert-huang transform and its applications*, (World Scientific, Singapore, 2005) Chap. 1, pp. 1–26.
- [44] P. A. Hwang, N. E. Huang, and D. W. Wang, *Appl. Ocean Res.* **25**, 187 (2003).
- [45] A. D. Veltcheva and C. G. Soares, *Appl. Ocean Res.* **26**, 1 (2004).
- [46] J. C. Echeverria, J. A. Crowe, M. S. Woolfson, and B. R. Hayes-Gill, *Med. Biol. Eng. Comput.* **39**, 471 (2001).
- [47] R. Balocchi, D. Menicucci, E. Santarcangelo, L. Sebastiani, A. Gemignani, B. Ghelarducci, and M. Varanini, *Chaos Soliton Fract.* **20**, 171 (2004).
- [48] V. I. Ponomarenko, M. D. Prokhorov, A. B. Bespyatov, M. B. Bodrov, and V. I. Gridnev, *Chaos Soliton Fract.* **23**, 1429 (2005).
- [49] N. E. Huang, M. L. Wu, W. Qu, S. R. Long, and S. S. P. Shen, *Appl. Stoch. Model Bus.* **19**, 245 (2003).
- [50] K. T. Coughlin and K. K. Tung, *Adv. Space Res.* **34**, 323 (2004).
- [51] I.M. Jánosi and R. Müller, *Phys. Rev. E* **71**, 56126 (2005).
- [52] M. K. I. Molla, M. S. Rahman, A. Sumi, and P. Banik, *Discrete Dyn. Nat. Soc.* **2006**, Article ID 45348, 17 pages (2006), doi:10.1155/DDNS/2006/45348.

- [53] J. Solé, A. Turiel, and J. Llebot, *Nat. Hazard Earth Sys. Sci.* **7**, 299 (2007).
- [54] Z. Wu, N. E. Huang, S. R. Long, and C. Peng, *PNAS* **104**, 14889 (2007).
- [55] C. H. Loh, T. C. Wu, and N. E. Huang, *BSSA* **91**, 1339 (2001).
- [56] J. Chen, Y. L. Xu, and R. C. Zhang, *J. Wind Eng. Ind. Aerodyn.* **92**, 805 (2004).
- [57] S. J. Loutridis, *Appl. Acoust.* **66**, 1399 (2005).
- [58] F. G. Schmitt, Y. Huang, Z. Lu, S. B. Zongo, J. C. Molinero, and Y. Liu, in *Nonlinear Dynamics in Geosciences*. edited by A. Tsonis and J. Elsner (Springer, 2007) pp. 261–280.
- [59] P. Flandrin, G. Rilling, and P. Gonçalvès, *IEEE Sig. Proc. Lett.* **11**, 112 (2004).
- [60] S. R. Long, N. E. Huang, C. C. Tung, M. L. Wu, R. Q. Lin, E. Mollo-Christensen, and Y. Yuan, *IEEE Geoscience and Remote Sensing Soc. Lett.* **3**, 6 (1995).
- [61] P. Flandrin, *Time-frequency/time-scale analysis* (Academic Press, 1998).
- [62] In fact, the Eq. (16) is convergence when $q \geq -1$. However, in practice, we only consider the case $q \geq 0$.
- [63] G. Rilling and P. Flandrin, *IEEE International Conference on Acoustics, Speech and Signal Processing, 2006. ICASSP 2006 Proceedings*. 2006 **3**, 444 (2006).
- [64] G. Rilling and P. Flandrin, *IEEE Trans. Signal Process* (2008).
- [65] G. Rilling and P. Flandrin, *Adv. Adapt. Data Anal.* **1**, 43 (2009).
- [66] D. Schertzer, S. Lovejoy, F. G. Schmitt, Y. Chigirinskaya, and D. Marsan, *Fractals* **5**, 427 (1997).
- [67] J. Schmittbuhl, F. G. Schmitt, and C. Scholz, *J. geophys. Res* **100**, 5953 (1995).
- [68] F. G. Schmitt, S. Lovejoy, and D. Schertzer, *Geophys. Res. Lett.* **22**, 1689 (1995).
- [69] P. Oświęcimka, J. Kwapien, and S. Drożdż, *Phy. Rev. E* **74**, 16103 (2006).
- [70] C. Heneghan and G. McDarby, *Phys. Rev. E* **62**, 6103 (2000).
- [71] Z. Chen, P. C. Ivanov, K. Hu, and H. E. Stanley, *Phys. Rev. E* **65**, 041107 (2002).
- [72] E. Koscielny-Bunde, J. Kantelhardt, P. Braun, A. Bunde, and S. Havlin, *J. Hydrol.* **322**, 120 (2006).
- [73] M. Sadegh Movahed, G. Jafari, F. Ghasemi, S. Rahvar, and M. Rahimi Tabar, *J. Stat. Mech.*, 02003 (2006).
- [74] J. Bardet and I. Kammoun, *Information Theory, IEEE Transactions on* **54**, 2041 (2008).
- [75] Q. Zhang, C. Xu, Y. Chen, and Z. Yu, *Hydrol. Process.* **22**, 4997 (2008).
- [76] S. Mallat and W. Hwang, *IEEE T. Inform. Theory.* **38**, 617 (1992).
- [77] S. Mallat, *A wavelet tour of signal processing* (Academic Pr, 1999).
- [78] H. Wendt, P. Abry, and S. Jaffard, *IEEE Signal Processing Mag.* **24**, 38 (2007).
- [79] I. Daubechies, *Ten lectures on wavelets* (Philadelphia: SIAM, 1992).
- [80] J. Beran, *Statistics for long-memory processes* (CRC Press, 1994).
- [81] L. Rogers, *Math. Finance* **7**, 95 (1997).
- [82] P. Doukhan, M. Taqqu, and G. Oppenheim, *Theory and Applications of Long-Range Dependence* (Birkhauser, 2003).
- [83] C. W. Gardiner, *Handbook of Stochastic Methods* (Springer, Berlin, third edition, 2004).
- [84] A. Wood and G. Chan, *J. Comput. Graph. Stat.* **3**, 409 (1994).
- [85] F. G. Schmitt, *Eur. Phys. J. B* **34**, 85 (2003).
- [86] E. Bacry, J. Delour, and J.F. Muzy, *Phys. Rev. E* **64**, 026103 (2001).
- [87] J.F. Muzy and E. Bacry, *Phys. Rev. E* **66**, 056121 (2002).
- [88] K. Sreenivasan, *Proc. R. Soc. Lond. A* **434**, 165 (1991).
- [89] B. Shraiman and E. Siggia, *Nature* **405**, 639 (2000).
- [90] Z. Warhaft, *Annu. Rev. Fluid Mech.* **32**, 203 (2000).
- [91] A. Celani, A. Lanotte, A. Mazzino, and M. Vergassola, *Phys. Rev. Lett.* **84**, 2385 (2000).
- [92] Y. Huang, F. G. Schmitt, and Y. Gagne, in preparation for *Phys. Rev. Lett.*
- [93] A. N. Kolmogorov, *Dokl. Akad. Nauk SSSR* **30**, 301 (1941).
- [94] A. Obukhov, *Izv. Acad. Nauk SSSR Ser. Geog. Geofiz* **13**, 58 (1949).
- [95] S. Corrsin, *J. Appl. Phys.* **22**, 469 (1951).
- [96] Z. S. She and E. Lévêque, *Phys. Rev. Lett.* **72**, 336 (1994).
- [97] W. van de Water and J. A. Herwijer, *J. Fluid Mech.* **387**, 3 (1999).
- [98] F. G. Schmitt, *Physica A* **368**, 377 (2006).
- [99] R.A. Antonia, E.J. Hopfinger, Y. Gagne, and F. Anselmet, *Phys. Rev. A* **30**, 2704 (1984).
- [100] G. Ruiz-Chavarria, C. Baudet, and S. Ciliberto, *Physica D* **99**, 369 (1996).
- [101] [Http://perso.ens-lyon.fr/patrick.flandrin/emd.html](http://perso.ens-lyon.fr/patrick.flandrin/emd.html).